Sulfuric Acid Improves the Reactivity of Zeolites *via* Dealumination

Xu Chen [1] and *Wil V. Srubar III* [1,2,†]

[1] Department of Civil, Environmental, and Architectural Engineering, University of Colorado Boulder, 1111 Engineering Drive ECOT 441 UCB 428, Boulder, Colorado USA 80309. [2] Materials Science and Engineering Program, University of Colorado Boulder, 4001 Discovery Drive, UCB 027, Boulder, Colorado USA 80303. [†] Corresponding Author: wsrubar@colorado.edu

Abstract

The demand for supplementary cementitious materials (SCMs), like fly ash, slag, and silica fume, is projected to rise over the next few decades. However, global decarbonization efforts, such as decommissioning of coal-fired power plants, will limit the supply of SCMs. Therefore, alternative SCM sources are a critical need for the cement and concrete industry. However, the high crystallinity of zeolites limits their pozzolanic reactivity. The goal of this work was to improve the reactivity of two common zeolites, namely clinoptilolite and SSZ-13, by treating them with sulfuric acid. The treatment enhanced zeolite reactivity *via* dealumination and decreased particle sizes, which led to increased reactivity with calcium hydroxide, as indicated by a 42.0% increase in reaction heat measured by isothermal calorimetry. We elucidate mechanistic understanding that smaller particle sizes induced by acid treatment accelerated peak heat evolution, while free aluminates from dealumination increased heat *via* direct reaction with aqueous Ca^{2+}.

Keywords: supplementary cementitious materials; zeolites; pozzolans; sulfuric acid.

1 Introduction

From a materials science perspective, supplementary cementitious materials (SCMs) improve both the sustainability and long-term durability of Portland cement concrete. Replacing proportions of cement with SCMs can achieve substantial reductions in CO_2 emissions [1, 2]. SCMs are also well known to densify the microstructure of Portland cement concrete *via* pozzolanic reactions, which improve transport properties and the long-term durability of concrete [3].

The demand for SCMs, like fly ash, slag, and silica fume [4], is projected to rise as global demand for cement is expected to rise to 6 Gt/year by 2050 [5]. The future supply of conventional SCMs, like fly ash, however, will be limited by global decarbonization efforts, such as the systematic decommissioning of coal-fired power plants [1]. A recent study reports that the majority of the global stockpiles of slag have been consumed [6]. Given the reductions in supply but increasefs in demand, a critical industry-wide need exists for identifying alternative viable sources of SCMs that exhibit sufficient pozzolanic reactivity [7, 8].

Zeolites, a family of crystalline aluminosilicate minerals, have the appropriate chemical composition to serve as alternative SCMs [1, 9, 10]. Widely available in nature [11], zeolites exhibit well-organized, high-surface-area nanostructures composed of silicon-oxygen and aluminum-oxygen tetrahedra [12]. Zeolites provide silicate and aluminate species that can react with calcium hydroxide (*i.e.,* $Ca(OH)_2$) to form calcium aluminosilicate hydrate (C-A-S-H) phases [13-15]. Researchers have reported that some zeolites can improve the strength and durability of Portland cement concrete [16-21]. Natural, untreated zeolites have been previously evaluated as pozzolans in many countries, including China, the United States, Russia, Cuba, and Germany [11, 22].

Despite these advances, early-age reactivity of zeolites has been a critical factor that hinders their widespread application in cementitious materials. Due to their high crystallinity, zeolites generally exhibit reactivity lower than most SCMs [23] but higher than some fly ashes [24]. Additionally, the strength of concrete has been shown to decrease when cement is replaced by zeolites in high percentages (>15%) especially at early ages (< 3 d) [24, 25].

Several methods have been employed to improve the reactivity of zeolites. The most common methods include milling, calcination, and acid treatment [14, 15, 26, 27]. Acid treatment has been found to improve zeolite reactivity *via* dealumination and simultaneous increases in specific surface area [26]. HNO_3, HCl, and acetic acid have been used to improve the pozzolanic activity of zeolites in cement paste [26]. In this study, the effects of dealumination and/or increased surface area were not necessarily distinguished from one another. As discussed in [26], treated zeolites when added directly to cement paste could nucleate additional hydration products from cement hydration, thereby confounding mechanistic interpretation of the enhanced reactivity. Other acids, including oxalic acid, citric

acid, and sulfuric acid, have been shown to dealuminate different types of zeolites [28-30], but corresponding enhancements of pozzolanic activity have not yet been studied.

In this study, two common zeolites, namely clinoptilolite and SSZ-13, were treated with sulfuric acid solutions. Clinoptilolite (Si/Al = 3.7 by mass) was treated with 0.1 M and 1.0 M sulfuric acid to investigate the changes in acid strength, a parameter that affects the erosion extent of cementitious materials [31]. SSZ-13 (Si/Al = 8.0 by mass) was treated with 0.1M sulfuric acid to investigate the effect of acid treatments on zeolites with different Si/Al ratios. Sulfuric acid was chosen based on previous work by the authors (and others) [32-35] that reported extensive sulfuric acid-induced dealumination of aluminosilicate frameworks. After acid treatment, resulting physical and chemical changes were investigated using scanning electron microscope (SEM), X-ray diffraction (XRD), nuclear magnetic resonance (NMR), and X-ray fluorescence (XRF). To examine effects on reactivity of zeolites, isothermal calorimetry tests were conducted on zeolite-laden pastes comprised predominantly of calcium hydroxide—a simpler system established in [36] that avoids any mechanistic obfuscation due to nucleation of reaction products that occurs during cement hydration. Furthermore, we discuss each of the physical and chemical effects on each stage of heat evolution, with an aim to provide a more thorough understanding on enhancement of reactivity that is induced by sulfuric acid treatment.

2 Materials and Experimental Methods

2.1 Materials

Natural clinoptilolite powders were purchased from KMI Zeolites (Pahrump, NV). SSZ-13 powder was obtained from ACS Materials (Pasadena, CA). Their chemical compositions were determined *via* XRF and summarized in **Table 1**. Sulfuric acid (H_2SO_4) was obtained from Macron Fine Chemicals. Calcium hydroxide (≥ 96.0%, Fluka Analytical), calcium carbonate (99 %, Acros Organics), potassium sulfate (≥ 99%, Sigma-Aldrich), and potassium hydroxide (≥ 85%, Fisher Scientific) were also obtained for the zeolite reactivity experiments.

Table 1 Chemical composition (wt. %), Si/Al ratio, and Na/Al ratio of raw clinoptilolite and SSZ-13. Elements (plus other trace metallic elements) are normalized to 100%.

Raw Zeolites	Al	Si	Na	Ca	Mg	K	Fe	S	Si/Al	Na/Al
Clinoptilolite	13.8	51.2	14.9	6.95	1.89	3.74	1.15	6.20	3.70	1.08
SSZ-13	11.0	88.4	-	0.11	-	0.10	0.21	0.17	8.00	-

2.2 Acid Treatment of Zeolites

For treatment, ~ 6 g of the powders was added to 150 ml of 0.1 M or 1 M sulfuric acid. The suspensions were kept stirring at room temperature (~ 20 °C) for 24 hours. The solid phase was then separated from the suspension by spinning at 10,000 rpm with an Eppendorf 5810R centrifuge. The obtained solid was washed by mixing with deionized water at a liquid/solid ratio of 10 and then separated by spinning at 10,000 rpm for 1 h. The wash process was repeated three times. The materials were dried under vacuum and deagglomerated gently with a mortar and pestle.

2.3 Physical and Chemical Characterization of Zeolites

Elemental analysis was performed in a Rigaku wavelength Dispersive (WD) XRF (Supermini200) spectrometer. A 200 W air-cooled Pd X-ray source operated at 50 kV and 4 mA was used to produce the excitation spectrum.

The physical and morphological properties of zeolites were characterized before and after treatment. Particle sizes were measured by a Malvern Mastersizer 3000 laser diffraction system with a measuring size range of 0.01-3500 μm. The morphology of the particles was examined using Hitachi SU3500 SEM instrument in secondary electron imaging mode. The instrument was operated between 10 and 15 kV. Prior to imaging, all samples were coated with ~10 nm of gold film under vacuum below 0.15 mb.

Crystal structures were characterized using a Siemens D500 and a Bruker D8 Advance XRD instrument. Powders of each sample were mixed with isopropyl alcohol, and a thin layer of the paste was casted on a Si crystal zero-background plate. Each sample was scanned using Cu Kα X-ray radiation from 5 to 45° 2θ with a step size of 0.02 and a dwell time of 1 s per step. The pattern was analyzed with the Diffrac.EVA software.

Nanostructures were probed by NMR using a Varian Inova 400 NMR spectrometer with a magnetic field of 9.4 T. For ^{27}Al NMR tests, a pulse of 3.1 μs was used. Recycle delay was 2 s and 2048 scans were acquired for each sample.

2.4 Pozzolanic Reactivity of Zeolite Pastes

Pozzolanic reactivity of zeolites before and acid treatment was assessed according to the established methodology previously reported in [36]. Mixture proportions are listed in **Table 2**. Each mixture was mixed with a Caframo Ultra Speed BDC6015 overhead stirrer at 140 rpm for 30 s and then at 285 rpm for 2.5 mins. In between the two speeded mixing, materials on the edges of the mixing cup were scraped.

Table 2 Mix design of pastes designed to assess pozzolanic reactivity (adapted from [36]).

Raw Materials	Zeolite	Portlandite ($Ca(OH)_2$)	Deionized water	KOH	K_2SO4	Calcite ($CaCO_3$)
Weight (g)	11.1	33.3	60.0	0.24	1.20	5.56

Reaction kinetics were monitored using Thermometric TAM Air 8-Channel Isothermal Conduction Calorimeter at 40ºC. Freshly mixed pastes (~14 g), composed of room-temperature water and cement, were weighed and placed into the glass ampoules for each sample. Siliceous sand (~ 14 g) was used as the reference material. The heat generated from the reaction was continuously recorded. The heat evolution and total heat were normalized by weight of zeolites.

3 Results and Discussion

3.1 Morphology and Particle Size

3.1.1 Morphology

Morphology of zeolites was examined using SEM (see **Fig. 1**). For the clinoptilolite, the raw (abbreviated as 'C'), 0.1 M acid treated ('C_0.1 M'), and 1 M acid treated ('C_1 M') samples in **Fig. 1(a, b, c)** exhibit both smooth (solid oval) and rough (dashed oval) particle surfaces. For the SSZ-13 in **Fig. 1(d, e)**, both the raw ('S') and 0.1 M acid-treated ('S_0.1 M') samples show a cubic-like morphology except the clear agglomerates (solid oval) for the raw SSZ-13 in **Fig. 1(d)**, suggesting that particle sizes decreased upon acid treatment. Overall, these two

zeolites exhibit minimum morphological changes after the acid treatment. The changes in particle sizes, crystallinity, and nanostructural characteristics are further examined in the following sections.

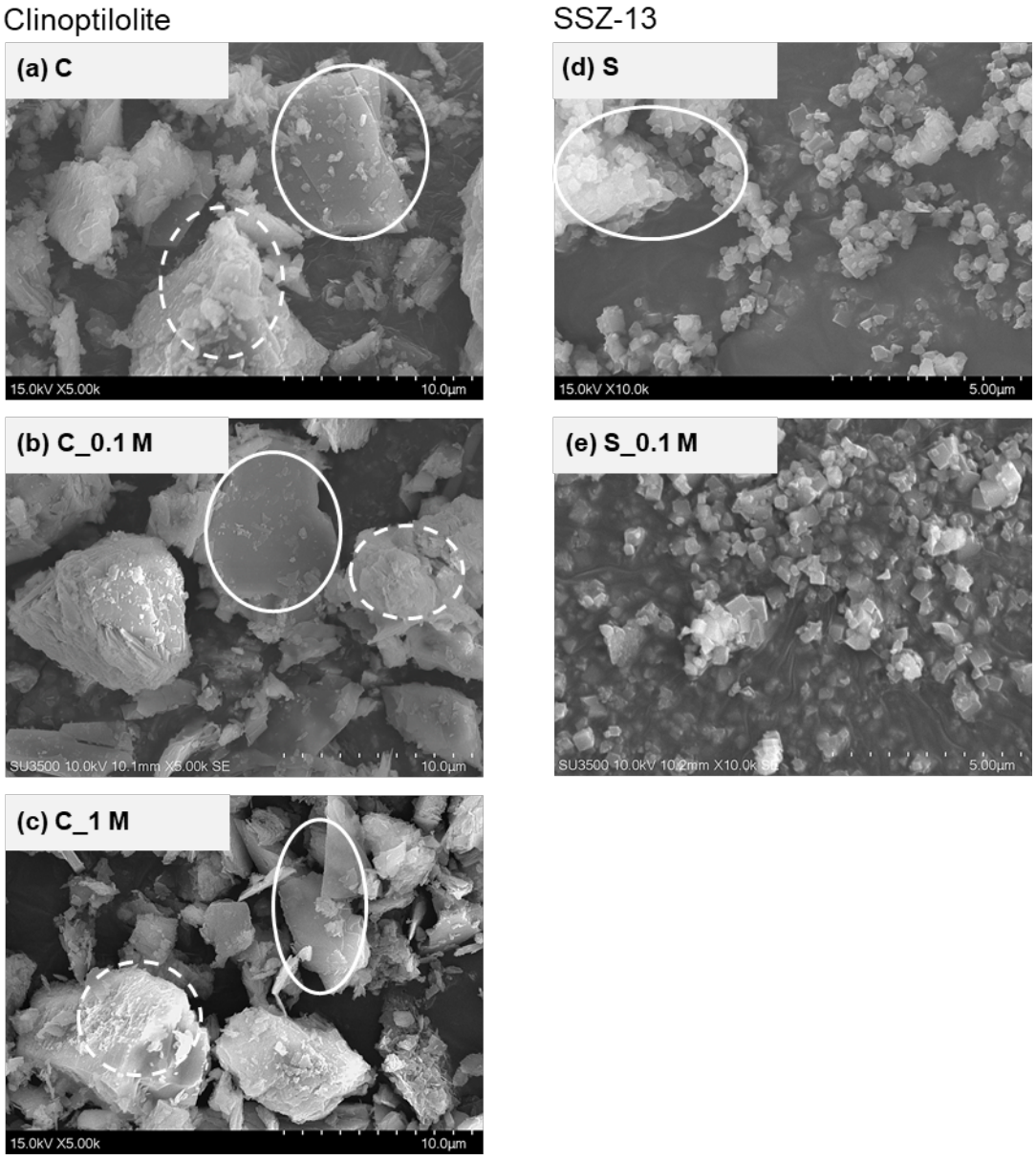

Fig. 1. SEM images of clinoptilolite (a) before and after treatment with (b) 0.1 M and (c) 1 M sulfuric acid, and SSZ-13 (d) before and (e) after 0.1 M acid treatment.

3.1.2 Particle Size

The particle sizes for both raw and acid-treated zeolites are reported in **Fig. 2**. For both clinoptilolite and SSZ-13, both size distribution and cumulative volume curves shifted to the

left, indicating that particle sizes decreased with acid treatment. A particle size average for each sample was calculated by summing the products of each size value (μm) with its corresponding percentage of size distribution. The average particle sizes of raw, 0.1 M, and 1 M acid treated clinoptilolite were 19.0, 6.9, 5.8 μm, respectively. Average particle size of raw and 0.1 M acid treated SSZ-13 were 20.7 and 9.6 μm, respectively. By comparison, the average particle size decreased by 63.7 and 69.5% upon 0.1 M and 1.0 M sulfuric acid treatment for clinoptilolite, and decreased by 53.6% upon 0.1 M acid treatment for SSZ-13. According to previously reported results, similar decreases in particle sizes of clinoptilolite were observed upon treatment with nitric acid and acetic acid, while hydrochloric acid reduced particle size to a lesser extent [26].

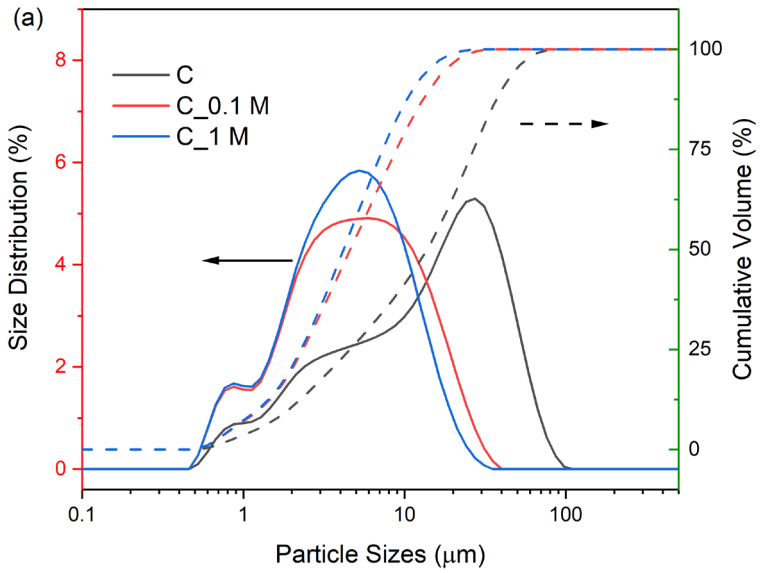

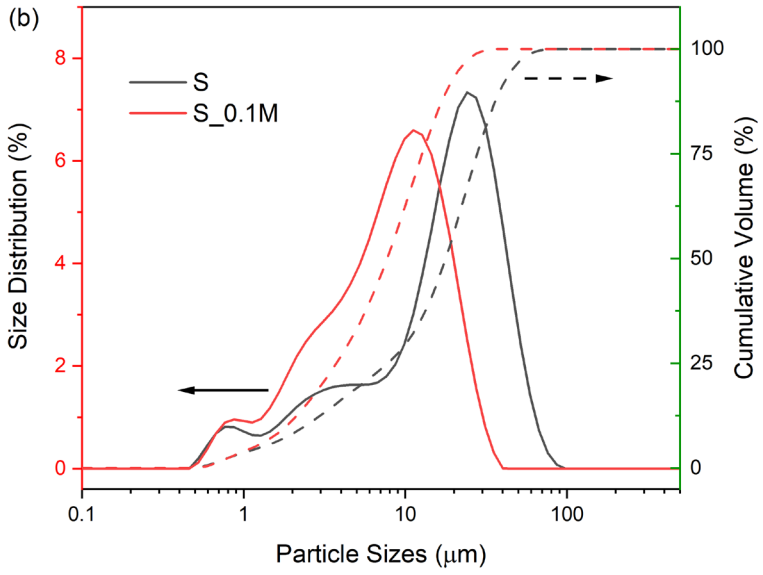

Fig. 2. Particle size distribution and cumulative curves (by volume) of raw and sulfuric acid-treated (a) clinoptilolite and (b) SSZ-13.

3.2 Structure

3.2.1 Crystallinity

The crystalline structures of clinoptilolite and SSZ-13 were altered after acid treatment, as indicated by the XRD patterns in **Fig. 3**. Results suggest that, while samples were not significantly amorphized by acid treatment, sulfuric acid likely removed cations, such as Na^+, and Al^{3+} from the aluminosilicate framework (*i.e.*, dealumination). For the clinoptilolite sample in **Fig. 3(a)**, some peak positions are altered, for instance in the rectangle-indicated peaks at round 22 (2θ), indicating a slight change in lattice spacing of the crystal structures upon the treatment of acid. A similar change in lattice parameters was observed in a dealuminated clinoptilolite in which Al vacancies weakened Si-O bonds and lengthened the Si-O distance [37]. Other minor crystallographic changes induced by acid treatment are evident in the intensity of clinoptilolite (marked as 'Cl') peaks (as indicated by rectangles). Similar intensity changes were observed for clinoptilolite samples upon dealumination by HCl [37] and can be attributed to the removal or exchange of cations [38] that results in a change of atomic density and atomic positions in the crystal structure [39, 40]. The removal of cations is evidenced by the reduced quantity of cations from XRF analysis, for example, in 0.1 M acid treated clinoptilolite in **Table A1** in the appendix. Additionally, the peak ~ 9.8 (2θ) is only broadened slightly, further suggesting no significant changes in crystallinity [37].

Other changes to the clinoptilolite samples include partial or full removal of gypsum and the formation of a new trace phase. The gypsum (GY) peaks were either reduced or removed after acid treatment (see **Fig. 3(a)**). However, the total weight percent of sulfur (S) is ~ 6%, and the percent change was trivial after acid treatment. For example, less than 1% change between 'C' and 'C_0.1 M' samples was observed (**Table A1**). Additionally, a new trace phase, namely tamarugite ($NaAl(SO_4)_2(H_2O)_6$), was identified in the 'C_1.0 M' sample. Given the limited quantity of both phases (*i.e.,* gypsum and tamarugite), however, they were unlikely to play a role in altering the reactivity of the zeolite sample.

For the SSZ-13 zeolite, changes induced by acid treatment are less evident (see **Fig. 3(b)**). The only observable change is the intensity of some peaks (as indicated by rectangles). This

change in intensity is not as substantial as that observed for clinoptilolite. SSZ-13 is charge balanced by H^+ as evidenced by minimum cations identified *via* XRF (**Table 1**), and its removal may have less of an effect on nanostructural stability compared to clinoptilolite (which is charge-balanced by Na^+). The lack of peak shift suggests less removal of Al^{3+} as compared to clinoptilolite that possesses a lower Si/Al ratio and, thus, is more susceptible to dealumination). In summary, while the 0.1 M sulfuric acid treatment reduces the average particle size of SSZ-13, evidence suggests it does not significantly alter its crystal structure.

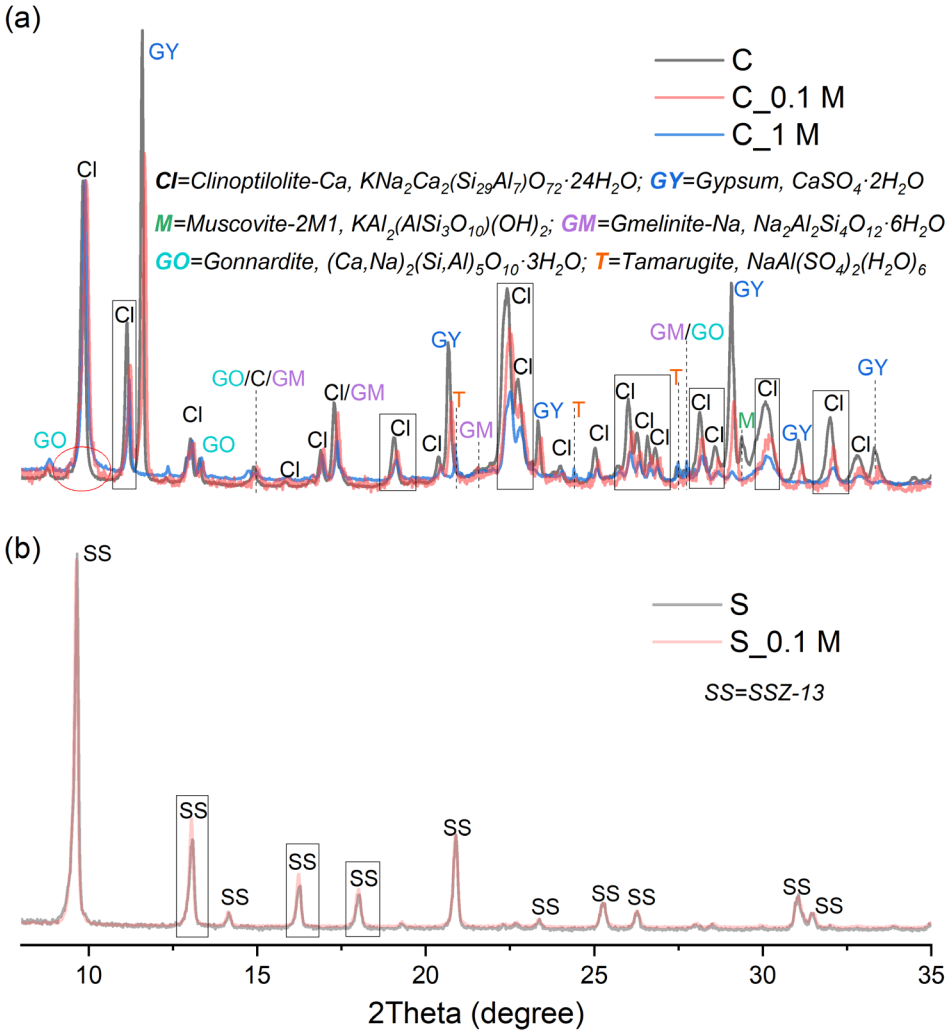

Fig. 3. XRD patterns of raw and acid-treated (a) clinoptilolite and (b) SSZ-13. PDF numbers: clinoptilolite-Ca (#00-039-1383), gypsum (#00-033-0311), muscovite-2M1 (#00-060-1516), gmelinite-Na (#00-038-0435), gonnardite (#00-042-1380), and tamarugite (#01-082-8691).

3.2.2 Nanostructures

Dealumination from the framework of both clinoptilolite and SSZ-13 was evident in the ^{27}Al NMR spectra (see **Fig. 4**), corroborating the XRD and XRF results. For clinoptilolite (see **Fig. 4(a)**), the increase of the 6-coordianted Al (abbreviated as 6-Al) peak (~0 ppm) upon acid treatment is attributed to the removal of Al from the framework [28-30]. When comparing 1.0 M to 0.1 M sulfuric acid-treated clinoptilolite, a higher intensity of 6-Al site was observed. Similarly, in an earlier study, high extent of dealumination from zeolite beta was observed only when treated with acid at 1 M or higher concentrations [41]. In addition, the 4-coordinated Al (abbreviated as 4-Al) peak (~60 ppm) was shifted to the right upon acid treatment. More explicitly, the 4-Al peak shifted from 60.0 ppm for the raw clinoptilolite to 58.3 ppm upon treatment with 1 M sulfuric acid. This shift indicates either a structural change from Q^4 to Q^3 or an increase in the Si/Al ratio. A change from Q^4 to Q^3 is unlikely, however, as it would have caused a more substantial shift in the spectra [42], thereby indicating that dealumination increased the framework Si/Al ratio, a finding that is consistent with the increase of the extra-framework Al (*i.e.*, 6-Al).

For SSZ-13 (**Fig. 4(b)**), a similar increase in 6-Al was observed, again indicating dealumination upon sulfuric acid treatment. No evident shift was observed for the 4-Al peak, because dealumination did not cause significant changes to the already high Si/Al ratio of SSZ-13 (see **Table 1**).

The sharp peak around -15 ppm for both types of zeolites after acid treatment (see **Fig. 4(a, b)**) was assigned to aluminum sulfate species with general formula $[Al(H_2O)_{6-x}(SO_4)_x]^{(3-2x)+}$ [43, 44]. Its relative low intensity in the ^{27}Al NMR spectra suggests (though not quantitatively) only trace amounts of this species. Such species could relate to the tamarugite phase identified in XRD.

From **Fig. 4**, the percentage of 6-Al for clinoptilolite increased 6% when treated with 0.1 M acid and by 46% when treated with 1.0 M acid. These percentage values are in reference to 4-Al as 100%. The percentage of 6-Al for SSZ-13 increased 33% when treated by 0.1 M acid. It is noted that these percent intensity values are not expected to be quantitative (*i.e.*, representative of the molar percent) due to the quadrupolar effects of the Al nucleus [45, 46].

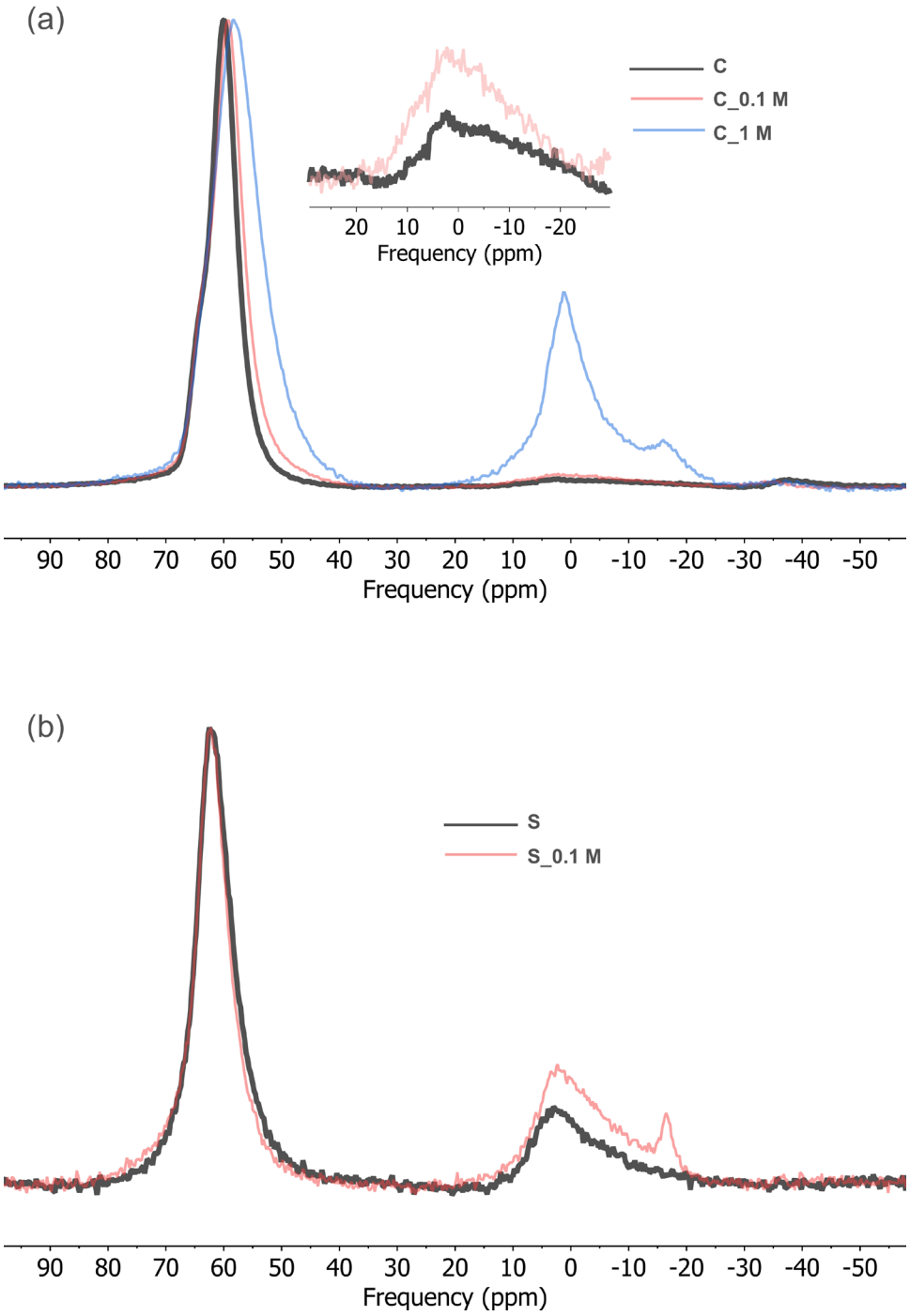

Fig. 4. ^{27}Al NMR spectra of raw and acid-treated (a) clinoptilolite and (b) SSZ-13.

3.3 Heat Evolution of Zeolite Pastes

In each heat evolution curve of the zeolite pastes (**Fig. 5**), three peaks are observed, namely peak A, B, and C in a consecutive order. In acid treated zeolite pastes, all these peak times

are accelerated, peak intensities are increased, and, correspondingly, the 24 h heat is increased, indicating acid treatment enhanced the pozzolanic reactivity of zeolites.

Peak A occurs immediately after mixing and is attributed to wetting and initial dissolution of particles. During wetting, water is adsorbed onto zeolites and can alter their unit-cell parameters [47]. This peak A is also attributable to the dissolution of $Ca(OH)_2$, an exothermal process that happens rapidly once the aqueous medium reaches pH 12.7 or above [48, 49]. As a result of this dissolution, deprotonation of the Si-OH and Al-OH bonds on the surface of the zeolites would likely occur [49].

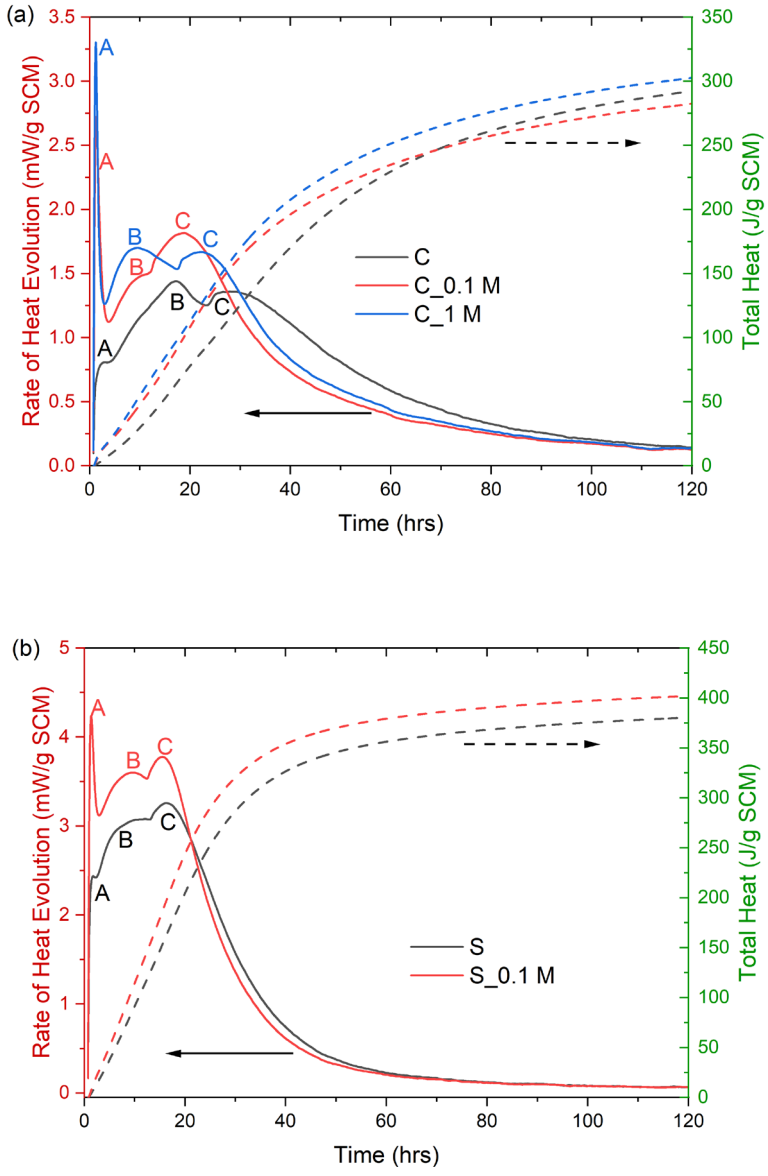

Fig. 5. Heat evolution and total cumulative heat for (a) clinoptilolite and (b) SSZ-13 zeolite pastes before and after the acid treatment.

Peak B can be attributed to the precipitation of surface-layer products. After reaching a supersaturated condition, the dissolved silicate and aluminate species react with Ca^{2+} to form precipitates. While the total quantity of the precipitates was found to be minimal at the end of Peak B in a similar zeolite-lime system [49], surface precipitation is likely to take place at the Si-O- and Al-O- sites on zeolite surfaces in a similar fashion as the reaction between surface silanol groups of a pozzolan and Ca^{2+} [50]. In such reaction, calcium silicate hydrate (C-S-H) and calcium-aluminate hydrate (C-A-H) phases are potential products [49, 51]. The semi-permeable surface products continue to grow as solution diffuses inward to further dissolve the zeolite to provide silicate and aluminate nutrients, a process that would release a substantial amount of heat [49].

Peak C is likely evidence of continuous reaction between the silicate and aluminate species from zeolites with $Ca(OH)_2$. This continuous precipitation has been confirmed by thermogravimetric analysis and XRD in a similar zeolite-lime system [49]. The transition from a surface precipitation (Peak B) to this continuous reaction (Peak C) could be explained by the protective-layer theory in cement hydration [52, 53], in which protective layers form on particle surfaces and eventually destabilize, promoting further hydration.

To understand the effects of sulfuric acid treatment on reactivity of the zeolites, the heat evolution values of Peaks A, B and C, as well as the total cumulative heat at different times (*i.e.*, 24 h and 100 h) are summarized in **Table 3**. Upon acid treatment, all peak times are accelerated, and all peak heat evolution values are increased. This observation indicates that sulfuric acid treatment enhanced reactivity of the zeolites at early ages (*i.e.*, within the first 20-30 h). Correspondingly, the 24 h heat was increased for all the pastes up to 42.0% for clinoptilolite and 15.9% for SSZ-13. Such extent of increase is higher than the ~10% increase in degree of hydration at 1 day in a cement-glass paste (75/25 by mass) at 50 ^{o}C as the glass particle sizes decreased from 25~ 38 μm to 0~25 μm [54]. Similar increases in peak heat were obtained at 100 h for all samples, aside from the 0.1 M-acid treated clinoptilolite sample, which exhibited a slight reduction compared to the untreated sample.

Table 3 Heat evolution values and peak times for Peaks A, B and C, as well as total heat at 24 and 100 h for pastes containing clinoptilolite and SSZ-13 zeolites before and after acid treatment.

Type of zeolite for pastes	Peak times of heat evolution (h)			Peak heat evolution (mW/g SCM)			24 h heat		100 h heat (J/g SCM)
	A	B	C	A	B	C	J/g SCM	% increase	
C (Raw)	2.7	17.1	27.9	0.81	1.44	1.36	96.3	-	280.1
C_0.1 M	1.3	10.4	18.5	2.72	1.49	1.82	133.2	38.3	272.2
C_1 M	1.3	9.2	22.4	3.31	1.70	1.67	136.8	42.0	291.8
S (Raw)	1.7	10.4	16.2	2.44	3.06	3.26	243.6	-	375.9
S_0.1 M	1.4	9.4	15.3	4.23	3.60	3.77	282.4	15.9	397.3

3.4 Mechanisms of Acid Treatment on the Reactivity

3.4.1 Reaction Heat

In **Fig. 6**, we plot the percent change upon acid treatment for heat evolution (Peak A, B and C), and 24 h and 100 h heat, average particle size, and 6-Al. Increased heat evolution and 24 h heat were found to correlate with decreased particle size, similar to earlier observations [15, 49, 55]. Their correlation, however, was not strong. For example, in **Fig. 6** the acid-treated SSZ-13, when compared to 'C_0.1 M', showed comparable decreases in the particle size but much lower changes in increased heat at 24 h. Decreased heat was observed at 100 h for 'C_0.1 M' contrary to the increased heat at 24 h. To understand the changes of reaction heat upon acid treatment, each stage of heat evolution will be discussed in detail with respect to the corresponding changes of both particle size and 6-Al in the next section.

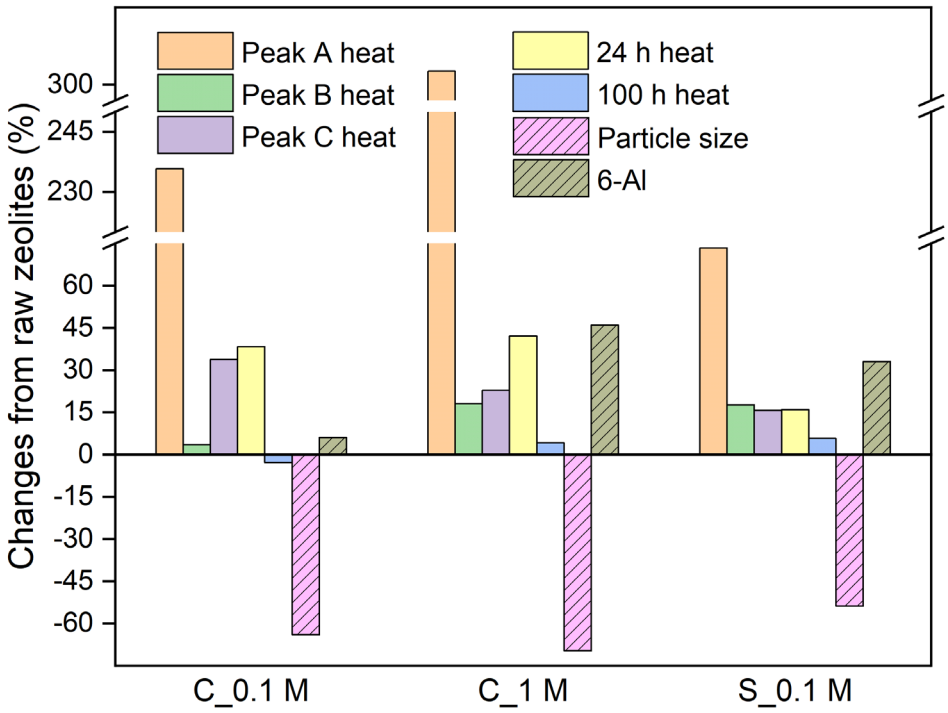

Fig. 6. Percent changes to peak heat evolution (Peak A, B, and C), 24 h cumulative heat, 100 h cumulative heat, 6-Al, and average particle size between raw and acid-treated clinoptilolite and SSZ-13 zeolites.

3.4.2 Stages of Heat Evolution

A schematic in **Fig. 7** summarizes the observable effects of sulfuric acid treatment on zeolites and resulting influence on heat evolution during different stages of reaction. Sulfuric acid treatment (I) decreased the particle sizes (as observed *via* particle size analysis), (II) removed the Al from the framework (based on NMR and as suggested by XRD observations), and (III) removed cations (as determined *via* XRD and XRF analysis). As indicated in the schematic, the first two changes (I, II) enhance heat evolution during the early stage (*i.e.*, peak A, B and C) while the third change (III) plays a role during the later stage. These effects are further discussed in detail.

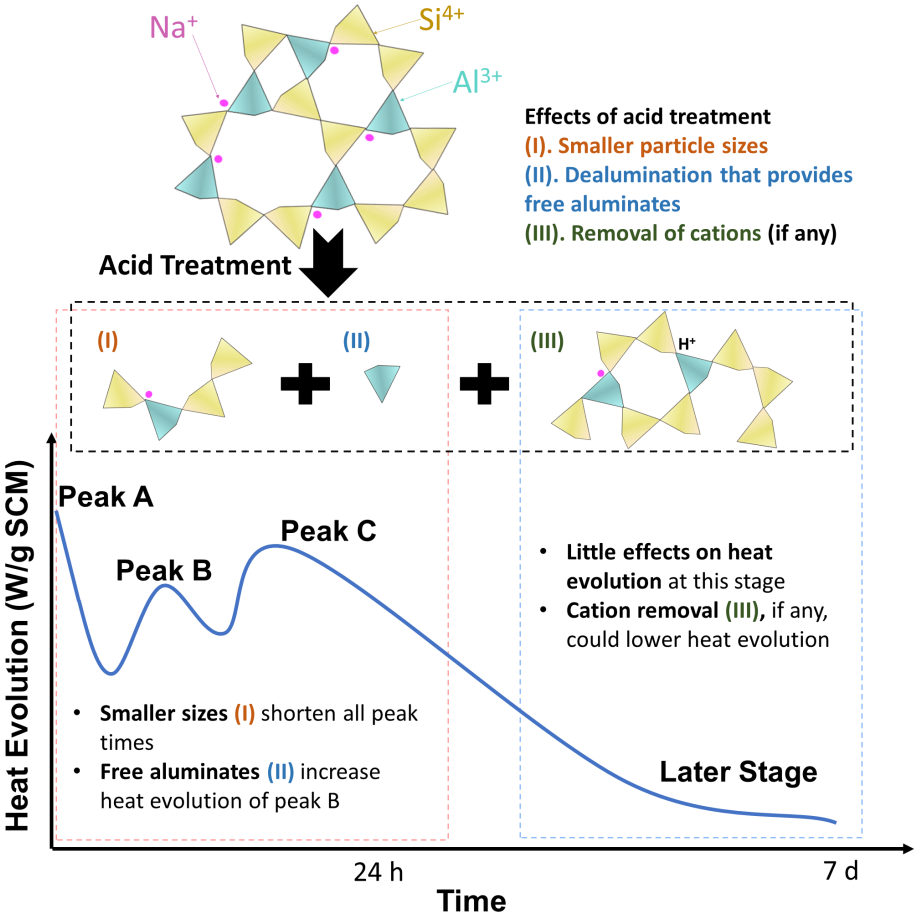

Fig. 7. Schematic for effects of acid treatment on zeolites, namely (I) smaller particles, (II) dealumination, and (III) removal of cations, and their influence on the heat evolution at early (Peak A, B and C) and later ages.

Peak A: The decrease of particle size was found to shorten peak time and increase heat evolution, while greater extent of dealumination yielded additional increases in heat evolution. As discussed, Peak A is attributed to initial wetting of the particles, dissolution of $Ca(OH)_2$, and corresponding deprotonation of Si-OH and Al-OH bonds. As shown in **Table 3**, the peak time decreased from 2.7 h to 1.3 h for acid-treated clinoptilolite, regardless of acid molarity. Peak time decreased from 1.7 h to 1.4 h for acid-treated SSZ-13. Heat evolution increased upon the acid treatment in all cases. These changes could be induced by the decreased particle sizes that provide more surface area for wetting and dissolution processes. However, the change in peak time did not necessarily correlate with dealumination. Peak times for 'C_0.1 M' and 'C_1 M' were identical, even though the extent of dealumination was substantially different (see **Fig. 4**). In contrast, the extent of

dealumination affects peak heat evolution. For example, the peak heat evolution increased from 2.72 to 3.31 mW/g SCM (see **Table 3**) with an increase in extent of dealumination (see **Fig. 4**) as acid molarity increased from 0.1 M to 1.0 M.

Peak B: The decrease in particle size was found to shorten peak time, while dealumination likely increased heat evolution associated with Peak B. By comparing 'C_0.1 M' with 'C' in **Table 3**, peak time was reduced from 17.1 to 10.4 h, but the peak heat evolution did not change (1.44 *vs*. 1.49 mW/g SCM). Peak time for the 'S_0.1 M' sample was reduced and peak heat evolution increased compared with 'S' (see **Table 3**). Given the substantial reductions in particle sizes upon acid treatment (**Fig. 2**), this observation indicated particle size more directly correlated with reductions in peak time for Peak B. In contrast, by comparing samples with increased dealumination extent (*i.e.*, 'C_1 M' *vs.* 'C_0.1 M' in **Fig. 4**), peak time did not vary, but the peak heat evolution increased 14.1% from 1.49 to 1.70 mW/g SCM. This observation indicated dealumination increased heat evolution. Besides providing free aluminates to directly react with Ca^{2+} to form C-A-H products [49, 51], dealumination produces Si-OH groups in zeolites [28], that would yield further increases in heat evolution *via* pozzolanic reaction with Ca^{2+} [56].

Peak C: Assigned herein as continuous precipitation, the peak time and heat evolution of Peak C depended on particle size and the characteristics of the prior peak (*i.e.*, Peak B). While reduced peak time and increased heat evolution of Peak C (**Table 3**) could be attributable to both particle size reduction and dealumination, dealumination was suggested to play a less critical role. This is evidenced by comparing the 'C_1 M' (higher dealumination) with 'C_0.1 M' that the peak time was delayed from 18.5 to 22.4 h and the peak heat evolution decreased from 1.82 to 1.67 mW/g SCM. Rather, the higher intensity of Peak B (*i.e.*, higher amount of precipitation) in 'C_1 M' likely hindered the continuous formation of precipitates and, thus, delayed and lowered the heat evolution of Peak C. This process is akin to cement hydration, in which accelerated early-age reaction and formation of protective layers of precipitates would retard reaction at later ages [52].

Later Stage (> 24 h): Reactions at later ages were unaffected by particle size or the presence of free aluminates but were influenced by the removal of cation upon the acid treatment. The 100 h heat decreased for 'C_0.1 M' compared to 'C', unlike the increase of the 24 h heat upon the acid treatment (**Table 3**). In a similar zeolite-lime reaction system, enhanced

reactivity at this relatively later stage (3 days or later) was found to depend on the cations in the zeolites [55]. These cations were released from the zeolites likely due to the relatively large framework apertures (*e.g.,* 3.0 × 7.6 Å; 3.3 × 4.6 Å; 2.6 × 4.7 Å for clinoptilolite framework [57]). This release (a process that generally consumes H^+) increased the pH of the aqueous phase and thus increased the solubility of the solids [49, 55]. However, such increased solubility is minimized in our pastes with acid-treated clinoptilolite, as most cations were removed during the acid treatment, as indicated by the XRD and XRF results (see Section 3.2.1). Unlike the clinoptilolite-laden pastes, the acid-treated SSZ-13 pastes showed a higher total heat throughout the tested period, likely because no cations are present in the initial SSZ-13 framework.

3.5 Significance

We have enhanced the early-age reactivity for clinoptilolite and SSZ-13 zeolites *via* a sulfuric acid treatment. Substantially high efficiency of this treatment has been suggested, given the 42.0% maximum increase of reaction heat at 24 hours observed for clinoptilolite. Such high efficiency would solve the issue of slow strength development for zeolite-laden cementitious pastes, which is a critical factor that hinders applications of zeolites as SCMs [24, 25].

This treatment can be applied to a variety of other zeolites, with the highest effectiveness for those with low Si/Al ratio, low cation (*e.g.,* Na^+ and K^+) content. Zeolites with lower Si/Al ratios possess relatively more Al sites for potential dealumination, which, as discussed above, increases the heat evolution. Furthermore, zeolites with low cation content are less susceptible to acid-induced removal of cations (which promote solid dissolution as discussed above).

Application of zeolites promises a large market share in the cement industry. Annual consumption of zeolite in China's cement industry was stated to be 30 million tons [24], a value that is much higher than another estimation of worldwide zeolite production in 2019 (*i.e.,* 1.2 million ton) [58]. However, this figure indirectly supports the claim of a substantially large worldwide reserve (though no specific value has been estimated) [58]. This 30 million ton capacity is comparable to the production of fly ash in 2018 in the United States (*i.e.,* 36.2 million tons) [59]. The cost of zeolites, dependent on the type and degree of processing, lies between \$50 ~ \$120 per ton (for powder sizes in 40 ~ 325 mesh) [60],

comparable to cement costs in the United States (*i.e.,* \$89.5 ~ \$123.5 per ton from 2007 to 2019) [61]. While sulfuric acid treatment introduces additional cost concerns, waste acid could be used in this treatment, as large quantities of sulfuric acid waste are generated in a variety of chemical and metal industries [62, 63]. Application of the sulfuric acid waste for such treatment would be next step of research.

4 Conclusions

In this study, we substantiated that early-age reactivity of zeolites can be improved *via* initial treatment with sulfuric acid. For both clinoptilolite and SSZ-13, treatment by sulfuric acid mainly (I) decreased particles sizes, (II) removed framework Al^{3+} through dealumination, and (III) removed cations, if any were initially present in the raw zeolite.

Reactivity was examined by calorimetry. The heat evolution curve exhibited three peaks: (Peak A) wetting and dissolution of particles, (Peak B) surface precipitation and associated dissolution and product formation, and (Peak C) continuous precipitation. Afterward, the reaction slowed, as anticipated. Upon acid treatment, all peaks occurred earlier and exhibited higher heat evolution at early ages (< 24 h).

We have shown detailed correlations between the changes induced by acid treatment and the resulting increase in the reactivity of the zeolites. Reduced particle size induced by acid treatment was found to shorten peak times for all the three peaks. While the reduced particle size helped increase the heat evolution of Peak A and C, the dealumination was found to more directly increase the heat evolution of Peak B. At later stages, such enhancing trend by acid treatment was not observed for the cation-containing zeolite (*i.e.,* clinoptilolite), probably because this trending was somewhat reversed by the acid-induced removal of cations.

The treatment developed in this study would substantially advance the performance, sustainability and cost efficiency of cementitious binders. The high efficiency of this treatment (*i.e.,* up to 42.0% increase in the early age reaction heat) substantially improves performance of the zeolite-laden cementitious binders. Considering the zeolites' abundant

reserve and comparable price to cements, this treatment, when applied to a variety of zeolites, exhibits a high potential benefit. Additional cost and environmental benefits could be addressed by the potential utilization of waste sulfuric acid to improve the reactivity of zeolites.

Acknowledgments

The work depicted was sponsored by the Advanced Research Projects Agency-Energy (Award Number: DE-AR0001145). Jorge Osio Norgaard's assistance with particle-size measurements in the Sedimentology Laboratory at the University of Colorado (CU) and Anastasia Aday's assistance with XRD at the United States Geological Survey are gratefully acknowledged. Centrifugation experiments were carried out with the help from Christine Marie Roberts in Dr. Chris Link's lab at the Institute for Behavioral Genetics at CU. Dr. Bimala Lama collected the NMR spectra at the NMR Spectroscopy Facility, SEM tests were conducted at the COSINC-Characterization Facility, and part of the XRD tests were conducted in geological science department, all at CU. Discussion on acid treatment and potential to use waste acids with Claire White at Princeton University is greatly appreciated. The XRF tests were performed at the Nebraska Nanoscale Facility, namely the National Nanotechnology Coordinated Infrastructure and the Nebraska Center for Materials and Nanoscience, which are supported by the National Science Foundation (Award No. ECCS-1542182) and the Nebraska Research Initiative. Any use of trade, firm, or product names was for descriptive purposes only and does not imply endorsement by the U.S. government.

References

[1] M.C.G. Juenger, R. Snellings, S.A. Bernal, Supplementary cementitious materials: New sources, characterization, and performance insights, Cem. Concr. Res. 122 (2019) 257-273.
[2] A. Souto-Martinez, E.A. Delesky, K.E.O. Foster, W.V. Srubar, A mathematical model for predicting the carbon sequestration potential of ordinary Portland cement (OPC) concrete, Cons. Build. Mater. 147 (2017) 417-427.
[3] K.A. Riding, M.D.A. Thomas, J.F. Kevin, Apparent diffusivity model for concrete containing supplementary cementitious materials, ACI Mater. J. 110 (2013) 705-714.

[4] B. Lothenbach, K. Scrivener, R.D. Hooton, Supplementary cementitious materials, Cem. Concr. Res. 41 (2011) 1244-1256.
[5] K.L. Scrivener, V.M. John, E.M. Gartner, Eco-efficient cements: potential economically viable solutions for a low-CO_2 cement-based materials industry, Cem. Concr. Res. 114 (2018) 2-26.
[6] R. Snellings, Assessing, understanding and unlocking Supplementary Cementitious Materials, RILEM Tech. Lett. 1 (2016).
[7] P. Suraneni, J. Weiss, Examining the pozzolanicity of supplementary cementitious materials using isothermal calorimetry and thermogravimetric analysis, Cem. Concr. Compos. 83 (2017) 273-278.
[8] P. Suraneni, T. Fu, V. Jafari Azad, O.B. Isgor, J. Weiss, Pozzolanicity of finely ground lightweight aggregates, Cem. Concr. Compos. 88 (2018) 115-120.
[9] B. Ahmadi, M. Shekarchi, Use of natural zeolite as a supplementary cementitious material, Cem. Concr. Compos. 32 (2010) 134-141.
[10] T. Perraki, E. Kontori, S. Tsivilis, G. Kakali, The effect of zeolite on the properties and hydration of blended cements, Cem. Concr. Compos. 32 (2010) 128-133.
[11] C. Colella, M.d. Gennaro, R. Aiello, Use of zeolitic tuff in the building industry, Rev. Miner. Geochem. 45 (2001) 551-587.
[12] A. Dyer, An introduction to zeolite molecular sieves, John Wiley and Sons Inc., New York, NY 1988.
[13] H.F.W. Taylor, Cement chemistry, Thomas Telford Services Ltd., Heron Quay, London 1997.
[14] S. Seraj, R.D. Ferron, M.C.G. Juenger, Calcining natural zeolites to improve their effect on cementitious mixture workability, Cem. Concr. Res. 85 (2016) 102-110.
[15] L.E. Burris, M.C.G. Juenger, Milling as a pretreatment method for increasing the reactivity of natural zeolites for use as supplementary cementitious materials, Cem. Concr. Compos. 65 (2016) 163-170.
[16] A.A. Ramezanianpour, R. Mousavi, M. Kalhori, J. Sobhani, M. Najimi, Micro and macro level properties of natural zeolite contained concretes, Cons. Build. Mater. 101 (2015) 347-358.
[17] R.E. Rodríguez-Camacho, R. Uribe-Afif, Importance of using the natural pozzolans on concrete durability, Cem. Concr. Res. 32 (2002) 1851-1858.
[18] I. Janotka, L. Krajči, Sulphate resistance and passivation ability of the mortar made from pozzolan cement with zeolite, J. Therm. Anal. Calorim. 94 (2008) 7-14.

[19] J.J. Chen, L.G. Li, P.L. Ng, A.K.H. Kwan, Effects of superfine zeolite on strength, flowability and cohesiveness of cementitious paste, Cem. Concr. Compos. 83 (2017) 101-110.
[20] C. Bilim, Properties of cement mortars containing clinoptilolite as a supplementary cementitious material, Cons. Build. Mater. 25 (2011) 3175-3180.
[21] C. Karakurt, İ.B. Topçu, Effect of blended cements produced with natural zeolite and industrial by-products on alkali-silica reaction and sulfate resistance of concrete, Cons. Build. Mater. 25 (2011) 1789-1795.
[22] N.Q. Feng, G.F. Peng, Applications of natural zeolite to construction and building materials in China, Cons. Build. Mater. 19 (2005) 579-584.
[23] M. Valipour, F. Pargar, M. Shekarchi, S. Khani, Comparing a natural pozzolan, zeolite, to metakaolin and silica fume in terms of their effect on the durability characteristics of concrete: a laboratory study, Cons. Build. Mater. 41 (2013) 879-888.
[24] C.S. Poon, L. Lam, S.C. Kou, Z.S. Lin, A study on the hydration rate of natural zeolite blended cement pastes, Cons. Build. Mater. 13 (1999) 427-432.
[25] F. Canpolat, K. Yılmaz, M.M. Köse, M. Sümer, M.A. Yurdusev, Use of zeolite, coal bottom ash and fly ash as replacement materials in cement production, Cem. Concr. Res. 34 (2004) 731-735.
[26] L.E. Burris, M.C.G. Juenger, The effect of acid treatment on the reactivity of natural zeolites used as supplementary cementitious materials, Cem. Concr. Res. 79 (2016) 185-193.
[27] T. Perraki, G. Kakali, E. Kontori, Characterization and pozzolanic activity of thermally treated zeolite, J. Therm. Anal. Calorim. 82 (2005) 109-113.
[28] Z. Yan, D. Ma, J. Zhuang, X. Liu, X. Liu, X. Han, X. Bao, F. Chang, L. Xu, Z. Liu, On the acid-dealumination of USY zeolite: a solid state NMR investigation, J. Mol. Catal. A: Chem. 194 (2003) 153-167.
[29] M.R. Apelian, A.S. Fung, G.J. Kennedy, T.F. Degnan, Dealumination of Zeolite β via dicarboxylic acid treatment, J. Phys. Chem. 100 (1996) 16577-16583.
[30] Y. Fan, X. Bao, X. Lin, G. Shi, H. Liu, Acidity adjustment of HZSM-5 zeolites by dealumination and realumination with steaming and citric acid treatments, J. Phys. Chem. B 110 (2006) 15411-15416.
[31] K. Yao, W. Wang, N. Li, C. Zhang, L. Wang, Investigation on strength and microstructure characteristics of nano-MgO admixed with cemented soft soil, Construction and Building Materials 206 (2019) 160-168.

[32] J.P. Gevaudan, A. Caicedo-Ramirez, M.T. Hernandez, W.V. Srubar, Copper and cobalt improve the acid resistance of alkali-activated cements, Cem. Concr. Res. 115 (2019) 327-338.
[33] J.P. Gevaudan, Mechanisms of biogenic acid degradation of low-calcium alkali-activated cements, Architectural Engineering, University of Colorado at Boulder, 2019
[34] C. Grengg, N. Ukrainczyk, G. Koraimann, B. Mueller, M. Dietzel, F. Mittermayr, Long-term in situ performance of geopolymer, calcium aluminate and Portland cement-based materials exposed to microbially induced acid corrosion, Cem. Concr. Res. 131 (2020) 106034.
[35] A. Allahverdi, F. Škvára, Sulfuric acid attack on hardened paste of geopolymer cements part 1. Mechanism of corrosion at relatively high concentrations, Ceram. Silik. 49 (2005) 225-229.
[36] X. Li, R. Snellings, M. Antoni, N.M. Alderete, M. Ben Haha, S. Bishnoi, Ö. Cizer, M. Cyr, K. De Weerdt, Y. Dhandapani, J. Duchesne, J. Haufe, D. Hooton, M. Juenger, S. Kamali-Bernard, S. Kramar, M. Marroccoli, A.M. Joseph, A. Parashar, C. Patapy, J.L. Provis, S. Sabio, M. Santhanam, L. Steger, T. Sui, A. Telesca, A. Vollpracht, F. Vargas, B. Walkley, F. Winnefeld, G. Ye, M. Zajac, S. Zhang, K.L. Scrivener, Reactivity tests for supplementary cementitious materials: RILEM TC 267-TRM phase 1, Mater. Struct. 51 (2018) 151.
[37] Y. Garcia-Basabe, I. Rodriguez-Iznaga, L.-C. de Menorval, P. Llewellyn, G. Maurin, D.W. Lewis, R. Binions, M. Autie, A.R. Ruiz-Salvador, Step-wise dealumination of natural clinoptilolite: structural and physicochemical characterization, Microporous Mesoporous Mater. 135 (2010) 187-196.
[38] F. Esenli, I. Kumbasar, X-Ray diffraction intensity ratios I(111)/I($3^{-}11$) of natural heulandites and clinoptilolites, Clays Clay Miner. 46 (1998) 679-686.
[39] P. Castaldi, L. Santona, S. Enzo, P. Melis, Sorption processes and XRD analysis of a natural zeolite exchanged with Pb^{2+}, Cd^{2+} and Zn^{2+} cations, J. Hazard. Mater. 156 (2008) 428-434.
[40] M.M. Woolfson, An introduction to X-ray crystallography, 2nd ed., Cambridge University Press, Cambridge, UK 1997.
[41] D.M. Roberge, H. Hausmann, W.F. Hölderich, Dealumination of zeolite beta by acid leaching: a new insight with two-dimensional multi-quantum and cross polarization ^{27}Al MAS NMR, Phys. Chem. Chem. Phys. 4 (2002) 3128-3135.

[42] C.I. Merzbacher, B.L. Sherriff, J.S. Hartman, W.B. White, A high-resolution ^{29}Si and ^{27}Al NMR study of alkaline earth aluminosilicate glasses, J. Non-Cryst. Solids 124 (1990) 194-206.
[43] A. Samadi-Maybodi, S.M. Pourali, M. Tafazzoli, Aluminum solvate complexes forming in acidic methanol-acetone mixtures studied by ^{27}Al NMR spectroscopy, J. Solution Chem. 38 (2009) 159-169.
[44] J.W. Akitt, J.A. Farnsworth, P. Letellier, Nuclear magnetic resonance and molar-volume studies of the complex formed between aluminium(III) and the sulphate anion, J. Chem. Soc., Faraday Trans. 1 81 (1985) 193-205.
[45] X. Chen, A. Sutrisno, L.J. Struble, Effects of calcium on setting mechanism of metakaolin-based geopolymer, J. Am. Ceram. Soc. 101 (2018) 957-968.
[46] X. Chen, A. Sutrisno, L. Zhu, L.J. Struble, Setting and nanostructural evolution of metakaolin geopolymer, J. Am. Ceram. Soc. 100 (2017) 2285-2295.
[47] R. Snellings, G. Mertens, S. Hertsens, J. Elsen, The zeolite–lime pozzolanic reaction: Reaction kinetics and products by in situ synchrotron X-ray powder diffraction, Microporous Mesoporous Mater. 126 (2009) 40-49.
[48] Z.Q. Wu, J.F. Young, The hydration of tricalcium silicate in the presence of colloidal silica, J. Mater. Sci. 19 (1984) 3477-3486.
[49] R. Snellings, G. Mertens, J. Elsen, Calorimetric evolution of the early pozzolanic reaction of natural zeolites, J. Therm. Anal. Calorim. 101 (2010) 97-105.
[50] N.Y. Mostafa, P.W. Brown, Heat of hydration of high reactive pozzolans in blended cements: Isothermal conduction calorimetry, Thermochim. Acta 435 (2005) 162-167.
[51] P.S. de Silva, F.P. Glasser, Hydration of cements based on metakaolin: thermochemistry, Adv. Cem. Res. 3 (1990) 167-177.
[52] D. Marchon, R.J. Flatt, 8 - Mechanisms of cement hydration, in: P.C. Aïtcin, R.J. Flatt (Eds.) Science and Technology of Concrete Admixtures, Woodhead Publishing, Cambridge, UK 2016, pp. 129-145.
[53] J.W. Bullard, H.M. Jennings, R.A. Livingston, A. Nonat, G.W. Scherer, J.S. Schweitzer, K.L. Scrivener, J.J. Thomas, Mechanisms of cement hydration, Cem. Concr. Res. 41 (2011) 1208-1223.
[54] M. Mirzahosseini, K.A. Riding, Influence of different particle sizes on reactivity of finely ground glass as Supplementary cementitious Material (SCM), Cem. Concr. Compos. 56 (2015) 95-105.

[55] G. Mertens, R. Snellings, K. Van Balen, B. Bicer-Simsir, P. Verlooy, J. Elsen, Pozzolanic reactions of common natural zeolites with lime and parameters affecting their reactivity, Cem. Concr. Res. 39 (2009) 233-240.
[56] N.Y. Mostafa, S.A.S. El-Hemaly, E.I. Al-Wakeel, S.A. El-Korashy, P.W. Brown, Characterization and evaluation of the pozzolanic activity of Egyptian industrial by-products: I: silica fume and dealuminated kaolin, Cem. Concr. Res. 31 (2001) 467-474.
[57] T. Armbruster, M.E. Gunter, Crystal structures of natural zeolites, Rev. Miner. Geochem. 45 (2001) 1-67.
[58] U.S. Geological Survey, Mineral commodity summaries 2020, U.S. Geological Survey, 2020, pp. 188-189.
[59] American Coal Ash Association, Coal combustion product production & use survey report, 2018.
[60] V.J. Inglezakis, A.A. Zorpas, Handbook of natural zeolites, Bentham Science Publishers, Sharjah, United Arab Emirates, 2012.
[61] Statista, Cement prices in the United States from 2007 to 2019, 2020.
[62] K. Song, Q. Meng, F. Shu, Z. Ye, Recovery of high purity sulfuric acid from the waste acid in toluene nitration process by rectification, Chemosphere 90 (2013) 1558-1562.
[63] J. Jeong, M.S. Kim, B.S. Kim, S.K. Kim, W.B. Kim, J.C. Lee, Recovery of H_2SO_4 from waste acid solution by a diffusion dialysis method, J. Hazard. Mater. 124 (2005) 230-235.

Appendix

Table A1 Chemical composition (wt%) of the raw and 0.1 M sulfuric acid treated clinoptilolite. Elements plus other trace metallic elements are normalized to 100%.

Zeolites	Al	Si	Na	Ca	Mg	S	K	Fe	**Si/Al**
C	13.83	51.20	14.91	6.95	1.89	6.20	3.74	1.15	**3.70**
C_0.1 M	13.17	59.12	7.61	6.49	1.56	6.09	4.47	1.46	**4.49**